SLAC-PUB-95-6764
October 1995

CALCULATIONS OF THE GIANT-DIPOLE-RESONANCE PHOTONEUTRONS USING A COUPLED EGS4-MORSE CODE

J. C. Liu, W. R. Nelson, K. R. Kase and X. S. Mao

Stanford Linear Accelerator Center, P. O. Box 4349, Stanford, CA 94309

Abstract - The production and transport of the photoneutrons from the giant-dipole-resonance reaction have been implemented in a coupled EGS4-MORSE code. The total neutron yield (including both the direct neutron and evaporation neutron components) is calculated by folding the photoneutron yield cross sections with the photon track length distribution in the target. Empirical algorithms based on the measurements have been developed to estimate the fraction and energy of the direct neutron component for each photon. The statistical theory in the EVAP4 code, incorporated as a MORSE subroutine, is used to determine the energies of the evaporation neutrons. These represent major improvements over other calculations that assumed no direct neutrons, a constant fraction of direct neutrons, monoenergetic direct neutron, or a constant nuclear temperature for the evaporation neutrons. It was also assumed that the slow neutrons (< 2.5 MeV) are emitted isotropically and the fast neutrons are emitted anisotropically in the form of $1+C\sin^2\theta$, which have a peak emission at 90°. Comparisons between the calculated and the measured photoneutron results (spectra of the direct, evaporation and total neutrons; nuclear temperatures; direct neutron fractions) for materials of lead, tungsten, tantalum and copper have been made. The results show that the empirical algorithms, albeit simple, can produce reasonable results over the interested photon energy range.

* Work supported by the U. S. Department of Energy under contract DE-AC-03-76SF00515.

A condensed version was presented at the 8th Symposium on Neutron Dosimetry in Paris, France, November 13-17, 1995

1. Introduction

At electron accelerators neutrons can be produced by bremsstrahlung photons through the giant-dipole-resonance (GDR), quasi-deuteron and photopion reactions. In the case of electron energy less than ~30 MeV (e.g., medical radiotherapy accelerators), the GDR photoneutron is the only source term. For low-power accelerator facilities (e.g., synchrotron light facilities) where the shields are generally thin, the GDR neutrons could be the dominant source. In these situations the spectral and angular distributions of the GDR photoneutrons are very important for many purposes, e.g., the shielding, the instrument response corrections for the neutron field measurements, etc.

Neutrons from the photon-induced GDR reaction consist of a large portion of evaporation neutrons which dominate at low energies (< 1-2 MeV) and a small fraction of direct neutrons which dominate at high energies. In this study, it is defined that the evaporation neutrons are emitted from an excited nucleus in an equilibrium state and the direct neutrons are emitted from all other states (e.g., the pre-equilibrium and 1p-1h states [1]). The energies of the evaporation neutrons can best be described by the Weisskopf's statistical model, on which the EVAP4 code [2,3] is based. The energies and yield of the direct neutrons can be calculated using the pre-equilibrium (or called pre-compound) theories, methods that the LAHET [4], ALICE [5], GNASH [6], and FLUKA [7] codes use. The evaporation neutrons are emitted isotropically and the emission of the direct neutron is peaked at 90° relative to the photon direction [1,8]. Note that there are some differences in the implementation of the pre-equilibrium theories among the codes. The ALICE and GNASH are actually only "cross section" generation codes. The FLUKA code is probably the only one that can treat the production and transport of the GDR neutrons, induced by photons, in a single code package [9]. In any case, to our knowledge, there has been no comprehensive presentations and verifications of the photoneutron spectra and angular distributions from these theoretical predictions.

On the other hand, calculations of the photoneutron spectra, using much more simplified assumptions, have been made for medical accelerators [10,11] or other applications [12,13]. These calculations suffer from the two major assumptions they used and, therefore, render their applications unsuitable for other situations, e.g., different targets and photon energies. The first assumption is the use of a Maxwellian fission spectrum with a constant nuclear temperature (T), regardless of the photon energy, to approximate an evaporation neutron spectrum [11,13]. However, it is known that the Maxwellian distribution actually fits only certain energy range of an evaporation neutron spectrum and a constant T value is appropriate only when the neutron energy is much smaller than the photon excitation energy. The second assumption is about the fraction and the spectral and angular distributions of the direct neutron component. For example, the spectral and angular distributions were assumed to be the same as those of the evaporation neutrons in [12,13], whereas the actual energy can be much higher [10,14]. The energy of the direct neutron was assumed to be the difference between the photon energy and the neutron separation energy in [10,11]. In the actual case, the direct neutron energies are smaller than the difference and they are not monoenergetic either. The fraction of the direct neutrons was assumed to be constant in [11], regardless of the target material and photon energy. In the actual case, the fraction should increase as the photon energy becomes higher, and should also varies for different target [14,15].

In this study, the implementation of the production and transport of the GDR photoneutrons, with regards to the spectral and angular distributions, in a coupled EGS4 and MORSE Monte Carlo code [16,17] is the main subject. The approach is a compromise between the abovementioned complicated and simplified methods, and the details of the approach will be described in Section 2. Basically, empirical algorithms were developed based mainly on the Mutchler thesis [14] to estimate the fraction and the energy of the direct neutron for each photon. The EVAP4 code, included as a subroutine of the MORSE, is used to obtain the energies of the evaporation neutrons. The emissions of the

neutrons $\leq$ 2.5 MeV are assumed to be isotropic and an angular algorithm, also derived from Mutchler [14], is used to obtain the anisotropic emissions of the neutrons > 2.5 MeV.

There are a few measurements about the spectral [14,15,18-23] and angular distributions [14,15,21-24] of the GDR neutrons for different beam (electron or photon) energies and target materials. The Mutchler thesis [14] gives the most comprehensive information and, therefore, was used as the main basis to derive the empirical algorithms. The photoneutron spectra calculated using this approach are compared with some measured spectra in Section 3, together with the discussions. The conclusions are given in the last section.

2. Methods

This section gives the details of the neutron yield calculation, the determination of the fractions and energies of the direct and evaporation neutron components, and the estimation of their emission angles. The materials of interest for this study are lead, tungsten, tantalum, and copper. Therefore, the empirical algorithms have been developed mainly based on the measurements made for these elements.

Outline

Figure 1 shows how an EGS4 user code UCPNCG MORTRAN and an input file UCPNCG DATA, using the Combinatorial Geometry (CG) routine, were used to generate a photon history file. The file contains the parameters of position (X_o, Y_o, Z_o), direction (U_o, V_o, W_o), energy (E_γ) and track length (l) for those photons capable of generating neutrons in each medium. Neutrons can be generated only in single-element media. The position of the neutron (X, Y, Z) was actually randomly sampled along the photon track. In the photon transport, attenuation due to the photonuclear reaction was ignored. This is

deemed acceptable, because the photonuclear cross section is at most a few percent of the atomic cross section. The neutron yield for each photon in a medium was calculated using the following probability estimator:

$$Y_j = \sum_{n=1}^{3} n\sigma_n \lambda B_j \rho / A \quad \text{for jth isotope} \qquad (1a)$$

where Y_j = neutron yield for jth isotope of the element in the medium,

n = number of neutrons per photoneutron generation (n=1-3),

σ_n = GDR photoneutron cross section to generate n neutrons,

l = photon track length,

B_j = abundance of isotope j,

ρ = density of the element,

A = atomic mass of the element,

The photoneutron cross sections σ_n, taken from the Atlas of Dietrich and Berman [25], are tabulated in a data file PNCROSS DATA, together with the parameters of B_j, ρ and A for each isotope. The total photoneutron yield from the EGS4 calculations is:

$$Y_{EGS} = \sum_{\gamma} \sum_{j} Y_{j\gamma} \qquad \text{for all photons and isotopes} \qquad (1b)$$

The use of the CG routine in the EGS4 allows not only complicated geometry modeling but also the coupling with the MORSE. The photon history file is then "read" by the MORSE with a user-written SOURCE subroutine, which has incorporated all the algorithms for photoneutron generation (see Fig. 2). A photon history was randomly sampled (block no. 4); the zone, medium and element were determined; and the neutron-

generation probability (P_j) and the yield (Y_j) for each isotope of the element were calculated. Because the EVAP4 determines neutron energy from each isotope, the atomic mass A_j and the neutron weight WT_j for each isotope were also calculated (block no. 3 in Fig. 2), using the probability fraction of each isotope PR_j. The total neutron yield (Y_s) for all sampled photons should agree with the Y_{EGS}, if there is an uniform sampling over all photon histories.

Direct Neutron

The fraction and energy of the direct neutron from each sampled photon are determined using the following empirical algorithms. The direct neutron fraction, F_d, is defined to be the ratio of the neutrons from the direct process to the total neutrons. Mutchler [14] defined his *measured* direct neutron fraction, F_m, as the ratio of the direct neutrons greater than 3 MeV to the total neutrons greater than 0.4 MeV. Figure 3 plots the measured direct neutron fraction (F_m) vs. the difference of the photon energy (E_γ) and the neutron separation energy (S_n) for a few high-Z isotopes from Mutchler [14]. It is known qualitatively [1,14,15] that the higher the photon energy, the higher the direct neutron fraction. In the photon energy range of interest, the maximum of the measured fractions [1,10,14,] was about 0.2. We further assumed that $F_d = F_m$ and only photons with energies greater than the S_n of the medium by 2.5 MeV can produce direct neutron. Therefore, a linear relationship shown in Fig. 3 was used as the algorithm to estimate the direct neutron fraction, F_d, as a function of photon energy:

$$F_d = 0, \qquad \text{for } (E_\gamma - S_n) < 2.5 \text{ MeV} \qquad (2a)$$

$$= 0.031(E_\gamma - S_n) - 0.077, \qquad \text{for } 2.5 \le (E_\gamma - S_n) \le 9 \text{ MeV} \qquad (2b)$$

$$= 0.2, \qquad \text{for } (E_\gamma - S_n) > 9 \text{ MeV} \qquad (2c)$$

The authors are aware of that the real function should be much more complicated. However, it will be shown in Section 3 that this simple algorithm is sufficient to predict reasonable direct neutron fractions for many cases. This simple algorithm is assumed to be applicable to all elements of interest. The weight of the direct neutron for each isotope is then $WT_j F_d$ and the weight for the evaporation neutron component is $WT_j(1-F_d)$. These will be assigned as the neutron weight (WATE) in the MORSE when each neutron is to be transported.

In the determination of the direct neutron energy, it was observed from the Mutchler thesis [14] that the direct neutron spectra from lead isotopes (undeformed nuclei) had peaks about 10-20% lower than the value of $(E_\gamma - S_n)$. The direct neutron spectra from tungsten and tantalum isotopes (deformed nuclei) were even softer. Therefore, for a photon with an energy E_γ and an isotope with a separation energy S_n, the resulting direct neutron intensity was assumed to be constant between the neutron energy values of $(E_\gamma - S_n)$ and $D(E_\gamma - S_n)$, where D is a constant. The direct neutron intensity was assumed to be zero at other energies. It will be demonstrated in Section 3 that D=0.7 for undeformed nuclei and D=0.4 for deformed nuclei would produce direct neutron spectra that are in fair agreement with the measured ones.

Evaporation Neutrons

The energies of the evaporation neutrons are determined using the statistical theory in the EVAP4 code. Because the EVAP4 may generate more than one neutron with different energies per photonuclear absorption, the weight of the evaporation neutron component, $WT_j(1-F_d)$, is to be shared by all evaporation neutrons produced.

To ensure that the evaporation neutron energies from the EVAP4 are correct, the level density parameters for the elements of interest in the EVAP4 were compared with the published values [26]. The agreements are within 10-20%, except for lead (due to ^{208}Pb, a double-magic nucleus), whose EVAP4 value is about 3 times higher. Therefore,

the level density parameter for lead in the EVAP4 was reduced to 2.5. As demonstrated in Section 3, the evaporation neutron spectra from the EVAP4 (with the change for lead) would have nuclear temperature values, for different materials and photon energies, in agreement with the measurements.

Neutron Emission Angle

Courant [8] has theoretically predicted that the angular distribution of the direct neutrons is in the form $1+C\sin^2\theta$, where θ is the angle between the incoming photon and the emitted neutron and C is a constant dependent on neutron energy. Figure 4 reproduces the measured relationship [14] between the constant C and the neutron energy for lead, tungsten and tantalum at different bremsstrahlung beam energies. To a first-order approximation, the relationship is not a function of photon energy and it can be described as the line shown in each subfigure; C=0 for slow neutrons, C rises to a maximum value of C_m, and then C remains constant up to the highest neutron enrergy, i.e., $(E_\gamma - S_n)$. The value C_m and the neutron energy E_c, at which the value C reaches its maximum, vary for different elements/isotopes. Due to the shell effects, fast neutrons from the ^{208}Pb isotope have the largest anisotropic emission (C_m=0.8 at E_c=7.6 MeV). The parameters of S_n from [10,14] and C_m and E_c from [14] for each isotope are also tabulated in the data file PNCROSS DATA.

In our angular algorithm, neutrons (either direct or evaporation) $\leq$ 2.5 MeV are assumed to be emitted isotropically, i.e., C=0. The linear line in each subfigure is used to estimate the value C at a neutron energy for an isotope. The function $1+C\sin^2\theta$ is then used to sample the neutron emission angle θ. Coordinate transformation is carried to obtain the direction cosines of the emitted neutron (U, V, W) from the angle θ and the photon angle (U_o, V_o, W_o). For isotopes (copper and iron) without measured angular distributions, the neutron emission is assumed to be isotropic.

3. Spectral Results and Comparisons

The validity of the neutron yield calculations has been checked satisfactorily against measurements in a previous report [27]. Because of the small fraction of fast neutrons and the scattering in the materials, the anisotropic emission of fast neutrons has only a small effect on the dose/spectra results at different directions. For example, the mean energies of the photoneutron spectra at 90° and 0° from a lead disk target (1.25 cm radius and 1.685 cm thick) bombarded by a 45-MeV electron beam were found to be only 1% difference. Therefore, in this section only the calculated photoneutron *spectra* are compared with the measurements for elements of lead, tungsten, tantalum and copper.

Lead

Using the time-of-flight technique, Mutchler [14] measured the photoneutron spectra from isotope targets of ^{208}Pb, ^{207}Pb and ^{206}Pb hit by bremsstrahlung beams with endpoints of 15, 14 and 13 MeV. Difference neutron spectra, resulting from an equivalent difference photon spectrum peaked at 14 (or 13) MeV with a FWHM of 2 MeV hitting each target, were obtained. By fitting the difference neutron spectra with the theoretical curves of the evaporation neutron and direct neutron components, Mutchler was able to separate the two neutron components and determine the spectra for both components. The difference photon spectrum peaked at 14 MeV is hereafter referred as the MIT 14 MeV photon beam.

The photoneutron spectrum from a lead disk target (2 cm radius and 0.635 cm thick) hit by the MIT 14 MeV photon beam [14] was calculated. The neutron yield ratios between the isotopes of ^{208}Pb, ^{207}Pb and ^{206}Pb were calculated to be 0.58:019:0.23, close to the corresponding isotope abundance ratio. The measured spectra for isotopes of ^{208}Pb, ^{207}Pb and ^{206}Pb were then weighted by the yield ratios to obtain the spectrum for the lead element. Spectral comparisons between the calculations and the measurements

are shown in Fig. 5a for direct neutrons and in Fig. 5b for total neutrons. The agreement of the direct neutron spectrum is quite satisfactory (note that the constant D in the algorithm is 0.7 for lead).

The semilogarithmic plot in Fig. 5b allows the determination of the nuclear temperature T from the slope of the evaporation neutron curve. With the adjustment of the level density parameter of lead in the EVAP4, the nuclear temperature T of the evaporation neutrons between 0.9-3.5 MeV is 0.97 MeV. This value is consistent with other published ones [14,15,23]. Figure 5b also shows that the calculated total spectrum is in good agreement with the Mutchler measurements (the two curves were arbitrarily normalized at 1.5 MeV), except at the high and low energy ends. The calculated F_m is 0.13, about 20% lower than the measured value of 0.16 [14]. The direct neutron fraction F_d is 0.12. It is important to note that, if without the inclusion of direct neutrons, the average energy of the neutron spectrum would be ~1.5 MeV, much smaller than the actual value of 2.28 MeV.

The photon track length distribution in the "thin" target from the MIT 14 MeV photon beam is quasi-monoenergetic. To check that the spectral algorithm can be applied to a much wider photon energy range, a comparison was made with the Kimura measurements [15]. One of the measurements that Kimura et al. made, using the time-of-flight technique, is the neutron spectrum at 90° with respect to the 16.5 MeV electron beam hitting a lead target (size 10x10x5 cm^3). In this "thick" target case the photon track length distribution in the target is close to E_γ^{-2} with a maximum of 16.5 MeV. The calculated neutron spectrum is shown in Fig. 6. The nuclear temperature value is 0.88 MeV for total neutrons between 2-3.5 MeV and is 1.45 MeV for total neutrons between 4-6 MeV. These calculated T values are within 3% of the measured ones, which again demonstrated our algorithms work. The calculated F_m and F_d are only 0.07 and 0.06, respectively, which are lower than the case of MIT 14 MeV beam. This can be expected, because the E_γ^{-2} photon track length distribution.

Tungsten

Tungsten element has four isotopes, but the photoneutron cross sections in [25] are available only for natural tungsten element and the ^{186}W isotope (only ~29% abundance). Therefore, the photoneutron cross sections for the tungsten element, instead of the four isotopes, were used to calculate neutron yield. On the other hand, the EVAP4 needs atomic mass for each isotope as an input to calculate the evaporation neutron energies. As shown in Fig. 7, the evaporation neutron spectra for all tungsten isotopes from the EVAP4 were found to be similar. Therefore, it was decided to use ^{184}W as the input to the EVAP4 for tungsten element.

The photoneutron spectrum from the MIT 14 MeV photon beam hitting a tungsten disk target, 2.54 cm radius and 0.556 cm thick, [14] was calculated. Spectral comparisons between the calculations and the measurements are shown in Fig. 8a for direct neutrons (with three D values) and in Fig. 8b for total neutrons. Considering the large uncertainty for the measured direct neutron spectrum, the empirical algorithm with a D=0.4 seems to produce a reasonable direct neutron spectrum. The nuclear temperature T for the evaporation neutrons between 0.9-3.5 MeV is 0.43 MeV. The calculated total spectrum is in fair agreement with the measurements, except again at the high and low energy ends. The calculated F_m is 0.15, about 15% higher than the measured value. The direct neutron fraction F_d is 0.13.

Another comparison with the measured photoneutrons from a tungsten target (1.8 cm radius and 2 cm thick) bombarded by a E_γ^{-1} bremsstrahlung beam with an endpoint of 24 MeV [26] was also made, and the results are shown in Fig. 9. The calculated nuclear temperature T is 0.49 MeV and the direct neutron fraction is 0.14. These values agree well with the measurements, which had a T value of 0.50 MeV by assuming a direct neutron fraction between 0.15-0.20.

Tantalum

The photoneutron cross sections for the ^{181}Ta isotope (~99.99% abundance) was used for the tantalum element. The photoneutron spectrum from the MIT 14 MeV photon beam hitting a tantalum disk target, 2.54 cm radius and 0.556 cm thick, [14] was calculated. Spectral comparisons between the calculations and the measurements are shown in Fig. 10a for direct neutrons (with three D values) and in Fig. 10b for total neutrons. Similar to the tungsten case, the algorithm with a D=0.4 produces a reasonable direct neutron spectrum. The nuclear temperature T for the evaporation neutrons between 0.9-3.5 MeV is 0.45 MeV, a value consistent with the published value of 0.49 MeV [26]. The calculated total spectrum is in fair agreement with the measurements, except at the high and low energy ends. The calculated F_m is 0.15, about 7% higher than the measured value [14]. The direct neutron fraction F_d is 0.13.

Copper

The empirical algorithms were developed based mainly on the Mutchler measurements, who measured the photoneutron spectra from isotopes with Z higher than 49. It is, therefore, important to check whether the algorithms are applicable to medium-Z elements, particularly for common target and shielding materials like copper and iron. Unfortunately, there are no good photoneutron spectral measurements for copper and iron.

However, two photoneutron measurements related to copper are available for comparison purpose. Using the nuclear emulsion films, Byerly and Stephen [21] measured a very crude photoneutron spectrum from a thin copper disk (0.32 cm radius and 0.635 cm thick) bombarded by a bremsstrahlung beam with an endpoint of 24 MeV. They estimated that the direct neutron fraction was ~0.1, with a neutron detection threshold of 0.3 MeV. The photoneutron spectrum from the Byerly and Stephen's copper experiment was calculated, and the results are shown in Fig. 11a for a E_γ^{-1} bremsstrahlung beam and

in Fig. 11b for a E_γ^{-2} beam. Note that, in the direct neutron spectral algorithm, the constant D is 0.7 for copper. The nuclear temperature T for the evaporation neutrons between 0.9-3.5 MeV is 0.74 MeV for a E_γ^{-1} bremsstrahlung beam and is 0.70 MeV for a E_γ^{-2} beam. The calculated direct neutron fraction (for neutrons higher than 0.3 MeV) is ~0.12-0.13, about 20-30% higher than the measured value.

Using a moderated BF_3 detection system, Barrett et al. [26] measured the mean energies of the photoneutron spectra from a copper disk (1.8 cm radius and 2 cm thick) bombarded by bremsstrahlung beams with varying endpoints. By assuming a direct neutron fraction of 0.15-0.20, they obtained a nuclear temperature of 1.0 MeV and a neutron mean energy of 1.78 MeV for a bremsstrahlung beam of 24 MeV. The photoneutron spectrum from the copper measurements of Barrett et al. was calculated, and the results are shown in Fig. 12 for a E_γ^{-1} bremsstrahlung beam with an endpoint of 24 MeV. The nuclear temperature T for the evaporation neutrons between 0.9-3.5 MeV is only 0.73 MeV, 27% lower than the measured value. However, the calculated mean energy for the total neutron spectrum is 1.88 MeV, only 6% higher than the measured. The calculated direct neutron fraction is 0.12.

4. Conclusions

For photons less than 30 MeV, the spectral and angular characteristics of the neutrons from the giant-dipole-resonance reaction are important for many applications. For example, the GDR photoneutrons contaminate seriously the radiation fields from medical accelerators operated above ~8 MeV. In the beamline shielding design for synchrotron light facilities, the GDR photoneutrons from gas bremsstrahlung hitting the beamline devices are one of the main radiation sources [28]. In this study the production and transport of the GDR photoneutrons for materials of interest for shielding design purposes have been implemented in a coupled EGS4-MORSE code. The total neutron

yield (including both the direct neutron and evaporation neutron components) is calculated by folding the photoneutron yield cross sections with the photon track length distribution in the target. Empirical algorithms based on the measurements have been developed to estimate the fraction and energy of the direct neutron component for each photon. The energies of the evaporation neutrons were determined using the statistical theory in the EVAP4 code, which is included as a subroutine of MORSE. It was also assumed that the slow neutrons ($\leq$ 2.5 MeV) are emitted isotropically and the fast neutrons are emitted anisotropically in the form of $1+C\sin^2\theta$, which have a peak emission at 90°.

General agreements between the calculated and the measured photoneutron results (spectra, nuclear temperatures and direct neutron fractions) for materials of lead, tungsten, tantalum and copper show that the simple algorithms can produce reasonable results over the interested photon energy range. The implementation of the angular algorithm showed small effects from the anisotropic emission of fast neutrons. Therefore, isotropic emission can be assumed for all neutrons without large error. The calculations in this study represent major improvements over those that assumed no direct neutrons, a constant fraction of direct neutrons, monoenergetic direct neutron, or a constant nuclear temperature for the evaporation neutrons. However, our approach may not be appropriate for elements with $Z < 20$, because of their more discrete features of the nuclear energy levels [19].

References

[1] A. Van Der Woude, Giant Resonances, Ch. 4 of the Prog. in Particle and Nuclear Physics, 18, edited by A. Faessler, Pergamon Press, N.Y. 267-273 (1987).

[2] ORNL, EVAP Calculation of Particle Evaporation from Excited Compound Nuclei, Radiation Shielding Information Center, Oak Ridge National Laboratory, PSR-10 (1974).

[3] I. Dostrovsky, Z. Fraenkel and G. Friedlander, "Monte Carlo calculations of nuclear evaporation processes, III. Applications to low-energy reactions", Phys. Rev. 116(3), 683-702 (1959).

[4] R. E. Prael and H. Lichtenstein, User Guide to LCS: The LAHET Code System, Los Alamos National Laboratory, LA-UR-89-3014 (1989).

[5] M. Blann, Recent Progress and Current Status of Preequilibrium Reaction Theories and Computer Code ALICE, Lawrence Livermore National Laboratory, UCRL-JC-109052 (1991).

[6] M. B. Chadwick and P. G. Young, Photonuclear Reactions in the GNASH Code: Benchmarking Model Calculations on Lead up to 140 MeV, Lawrence Livermore National Laboratory, UCRL-ID-118721 (1994).

[7] A. Ferrari and P. R. Sala, "A new model for hadronic interactions at intermediate energies for the FLUKA code", Proc. of the MC93 Int. Conf. on Monte Carlo Simulation in High-Energy and Nuclear Physics, Tallahassee, FL, February 22-26 (1993).

[8] E. D. Courant, "Direct photodisintegration process in nuclei", Phys. Rev. 82(5), 703-709 (1951).

[9] A. Fasso, A. Ferrari and P. R. Sala, "Designing electron accelerator shielding with FLUKA", Accelerator Shielding Specialist Meeting, Arlington, TX, April (1994).

[10] NCRP, Neutron Contamination from Medical Electron Accelerators, National Council on Radiation Protection and Measurements, Bethesda, MD, NCRP Report 79 (1984).

[11] S. Agosteo, A. Foglio Para, M. Silari, A. Torresin and G. Tosi, "Monte Carlo simulations of neutron transport in a linac radiotherapy room", Nucl. Instru. Meth. in Phys. Res. B72, 84-90 (1992).

[12] T. W. Armstrong, B. L. Colborn and D. L. Johnson, "Transport calculations of radiation streaming through shielding penetrations for a free-electron-laser accelerator facility", Proc. of the ANS Topical Meeting on New Horizons in Radiation Protection and Shielding, Pasco, WA, April 26-May 1 (1992).

[13] T. W. L. Sanford, L. J. Lorence, J. A. Halbleib, J. G. Kelly, P. J. Griffin, J. W. Poukey, W. H. McAtee and R. C. Mock, "Photoneutron production using bremsstrahlung from the 14-TW pulsed-power HERMES III electron accelerator", Nucl. Sci. and Eng. 114, 109-213 (1993).

[14] G. S. Mutchler, The Angular Distributions And Energy Spectra of Photoneutrons from Heavy Elements, Ph.D. Thesis, Massachusetts Institute of Technology (1966).

[15] I. Kimura, S. A. Hayashi, K. Kobayashi, S. Yamamoto and T. Shibata, "Measurements of angular distributions and energy spectra of photoneutrons from lead targets bombarded by high energy electrons", Ann, Repts. of Res. Reactor Inst. Kyoto Univ. 3, 75-83 (1970).

[16] W. R. Nelson, H. Hirayama and D. W. O. Rogers, The EGS4 Code System, Stanford Linear Accelerator Center, SLAC-265 (1985).

[17] M. B. Emmett, The MORSE Monte Carlo Radiation Transport Code System, Radiation Shielding Information Center, Oak Ridge National Laboratory, ORNL-4972 (1975).

[18] R. F. Askew and A. P. Batson, "Energy spectrum of the photoneutrons from gold", Nucl. Phys. 20, 408-416 (1960).

[19] F. W. K. Firk, "Energy spectra of photoneutrons from the reactions $O^{16}(\gamma,n)$, $S^{32}(\gamma,n)$ and $Ca^{40}(\gamma,n)$", Nucl. Phys. 52, 437-448 (1964).

[20] F. T. Kuchnir, P. Axel, L. Criegee, D. M. Drake, A. O. Hanson and D. C. Sutton, "Neutron spectra from monoenergetic photons on bismuth", Phys. Rev. 161(4), 1236-1248 (1967).

[21] P. R. Byerly, Jr. and W. E. Stephens, "Photodisintegration of copper", Phys. Rev. 83(1), 54-62 (1951).

[22] M. E. Toms and W. E. Stephens, "Photoneutrons from lead", Phys. Rev. 108(1), 77-81 (1951).

[23] D. B. Gayther and P. D. Goode, "Neutron energy spectra and angular distributions from targets bombarded by 45 MeV electrons", Journal of Nucl. Energy. 21, 733-747 (1967).

[24] H. L. Poss, "Note on angular asymmetries in (γ,n) reactions", Phys. Rev. 79, 539-540 (1950).

[25] S. S. Dietrich and L. B. Berman, "Atlas of photoneutron cross sections obtained with monoenergetic photons", At. Data Nucl. Data Tables, 38, 199 (1988).

[26] R. F. Barrett, J. R. Birkelund, B. J. Thomas, K. S. Lam and H. H. Thies, "Systematic of nuclear level density parameters of nuclei deficient in one neutron", Nucl. Phys. A210, 355-379 (1973).

[27] X. Mao, K. R. Kase, and W. R. Nelson, "Giant-Resonance neutron yields as functions of materials and thickness of the targets struck by electrons", Stanford Linear Accelerator Center, Stanford, CA, SLAC-PUB-6628 (1994).

[28] J. C. Liu, W. R. Nelson and K. R. Kase, "Gas bremsstrahlung and associated photon-neutron shielding calculations for electron accelerators", Health Phys. 68(2), 205-213 (1995).

Captions of Figures

Figure 1. An EGS4 user code, using the Combinatorial Geometry (CG) routine, was used to generate a photon history file which contains the parameters of position (X_o, Y_o, Z_o), direction (U_o, V_o, W_o), energy (E_γ) and track length (l) for those photons capable of generating neutrons in the media. The neutron yield for each photon is calculated by folding the photon track length with the photoneutron yield cross sections.

Figure 2. The flow chart for the generation and transport of the photoneutrons using the SOURCE subroutine of the MORSE, which included the EVAP4 as one of the subroutines. See text for detailed description.

Figure 3. The direct neutron fraction vs. the difference of the photon energy (E_γ) and the neutron separation energy (S_n) for a few high-Z isotopes, measured by Mutchler [14]. The linear line shown was used as the function to estimate the direct neutron fraction.

Figure 4. The angular distribution of the photoneutrons is in the form $1+C\sin^2\theta$, where θ is the angle between the incoming photon and the emitted neutron and the constant C is a function of neutron energy. The measured relationship [14] between the constant C and the neutron energy for lead, tungsten and tantalum at different photon energies are reproduced here. The relationship is approximated as the line shown in each subfigure.

Figure 5. Spectral comparisons between the calculations and the measurements [14] for direct neutrons (part a) and total neutrons (part b) from a lead target hit by the MIT 14 MeV photons. The nuclear temperature T determined from the slope of the evaporation neutron curve (in the neutron energy of 0.9-3.5 MeV) is 0.97 MeV. The calculated total spectrum also agrees with the measurement,

except at the high and low energy ends. The calculated F_m is 0.13, about 20% lower than the measured value, and the direct neutron fraction F_d is 0.12.

Figure 6. Calculated neutron spectrum at 90° relative to a 16.5 MeV electron beam hitting a thick lead target (10x10x5 cm^3). The nuclear temperature T values for two neutron energy regions are within 3% of the measured ones [15].

Figure 7. Evaporation neutron spectra for four tungsten isotopes calculated by the EVAP4.

Figure 8. Spectral comparisons between the calculations and the measurements [14] for direct neutrons (part a) and total neutrons (part b) from a tungsten target hit by the MIT 14 MeV photons. The algorithm with a D=0.4 gives a reasonable direct neutron spectrum. The nuclear temperature T for the evaporation neutrons between 0.9-3.5 MeV is 0.43 MeV. The calculated total spectrum is in fair agreement with the measurements, except at the high and low energy ends. The calculated F_m is 0.15, about 15% higher than the measured value, and the direct neutron fraction F_d is 0.13.

Figure 9. Calculated photoneutrons from a tungsten target (1.8 cm radius and 2 cm thick) bombarded by a E_γ^{-1} bremsstrahlung beam with an endpoint of 24 MeV. The calculated nuclear temperature T is 0.49 MeV and the direct neutron fraction is 0.14, which agree well with the measurements [26].

Figure 10. Spectral comparisons between the calculations and the measurements [14] for direct neutrons (part a) and total neutrons (part b) from a tantalum target hit by the MIT 14 MeV photons. The algorithm with a D=0.4 gives a reasonable direct neutron spectrum. The nuclear temperature T for the evaporation neutrons between 0.9-3.5 MeV is 0.45 MeV. The calculated total spectrum is in fair agreement with the measurements, except at the high and low energy ends. The calculated F_m is 0.15, about 7% higher than the measured value, and the direct neutron fraction F_d is 0.13.

Figure 11. Photoneutron spectrum from a copper disk (0.32 cm radius and 0.635 cm thick) bombarded by a bremsstrahlung beam with an endpoint of 24 MeV; a) E_γ^{-1} bremsstrahlung beam and b) E_γ^{-2} beam. Note the small difference of the nuclear temperature.

Figure 12. Photoneutron spectrum from a copper disk (1.8 cm radius and 2.0 cm thick) bombarded by a E_γ^{-1} bremsstrahlung beam with an endpoint of 24 MeV.

EGS4 User Code: UCPNCG MORTRAN

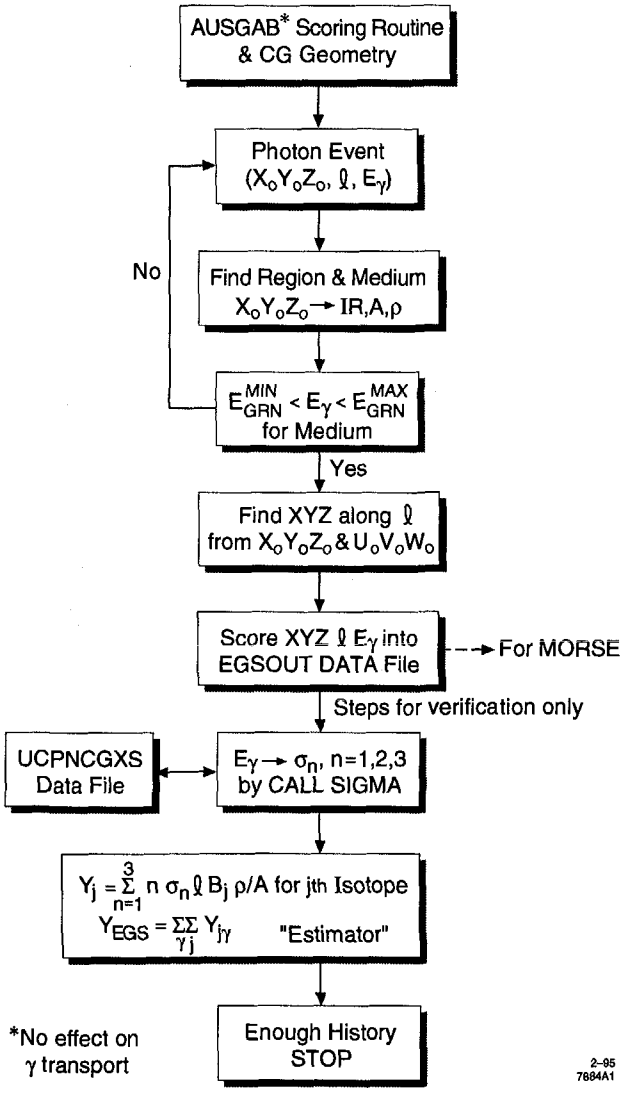

Fig. 1

MORSE User Code: MORSGRN FORTRAN

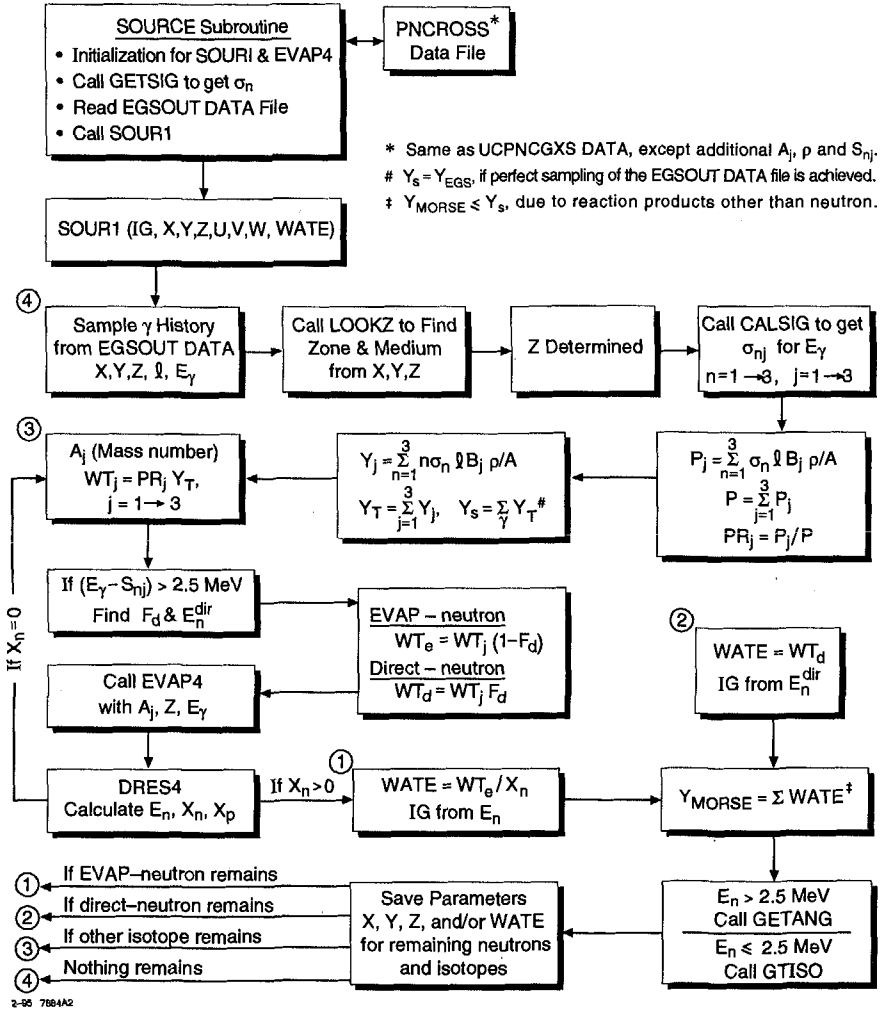

Fig. 2

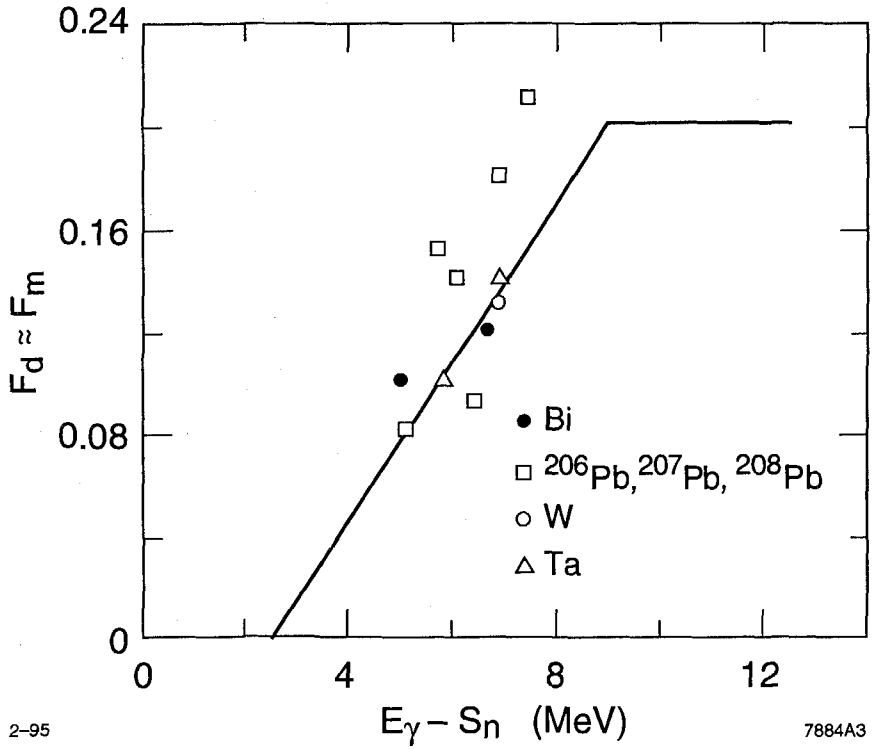
0.24
0.16
0.08
0
$F_d \approx F_m$
0
4
8
12
$E_\gamma - S_n$ (MeV)
● Bi
□ ^{206}Pb, ^{207}Pb, ^{208}Pb
○ W
△ Ta
2–95
7884A3

Fig. 3

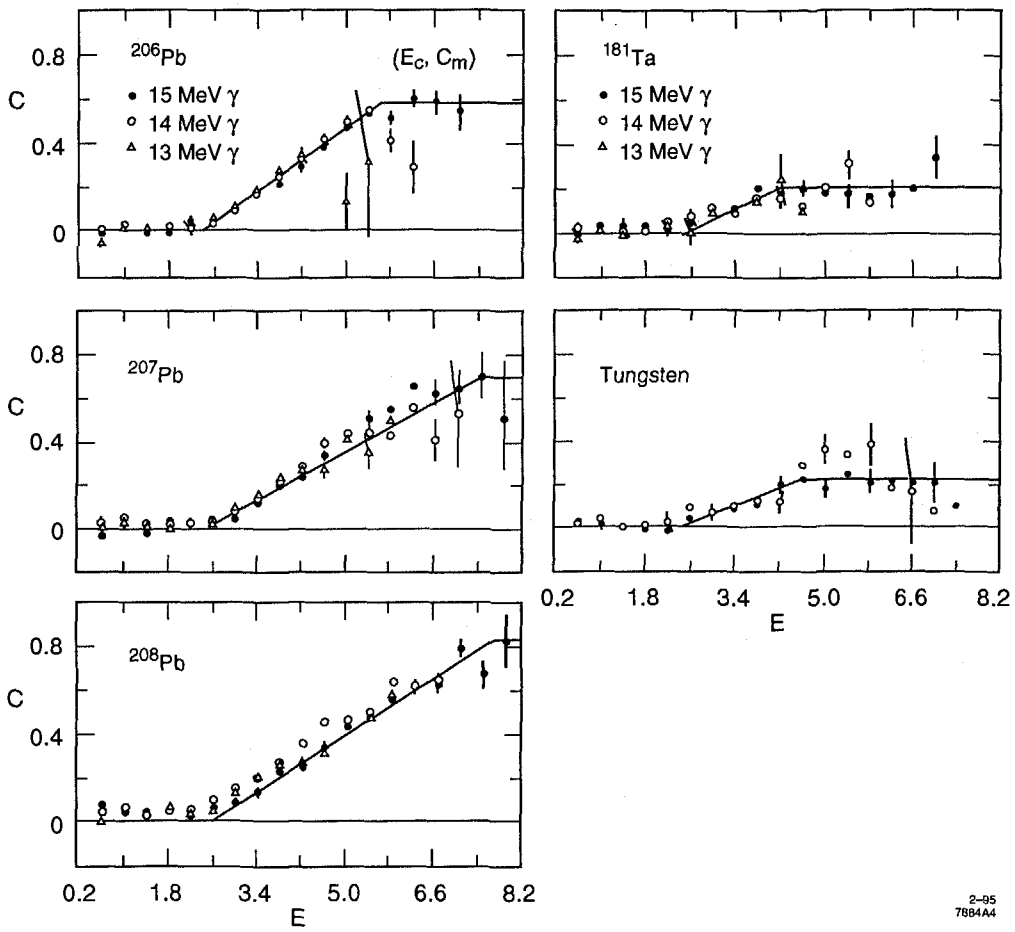
^{206}Pb
(E_c, C_m)
• 15 MeV γ
○ 14 MeV γ
△ 13 MeV γ
^{181}Ta
^{207}Pb
Tungsten
^{208}Pb
C
0.8
0.4
0
0.2
1.8
3.4
5.0
6.6
8.2
E
2–95
7884A4

Fig. 4

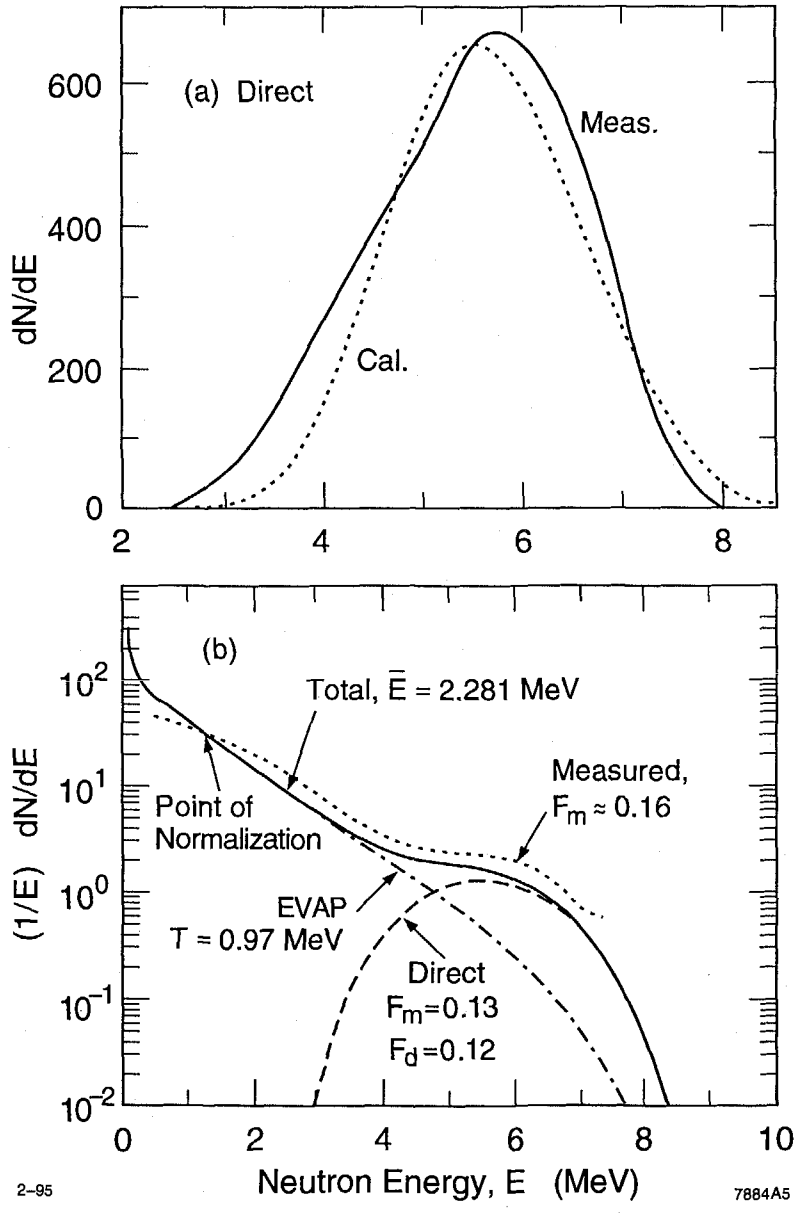
(a) Direct
Meas.
Cal.
dN/dE
600
400
200
0
2
4
6
8
(b)
Total, $\bar{E}$ = 2.281 MeV
Measured,
$F_m \approx 0.16$
Point of
Normalization
EVAP
T = 0.97 MeV
Direct
F_m=0.13
F_d=0.12
(1/E) dN/dE
10^2
10^1
10^0
10^{-1}
10^{-2}
0
2
4
6
8
10
Neutron Energy, E (MeV)
2-95
7884A5

Fig. 5

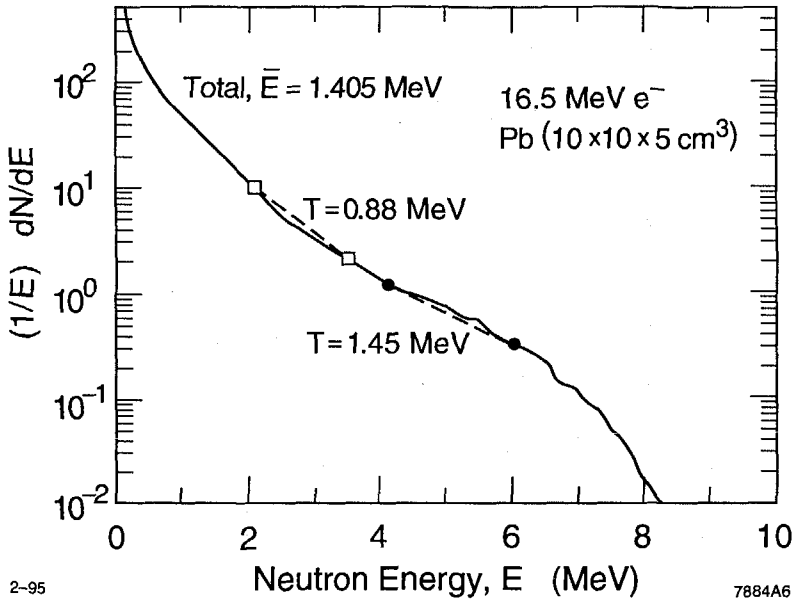
Total, $\bar{E}$ = 1.405 MeV
16.5 MeV e^-
Pb (10 x 10 x 5 cm^3)
T = 0.88 MeV
T = 1.45 MeV
(1/E) dN/dE
10^2
10^1
10^0
10^{-1}
10^{-2}
0
2
4
6
8
10
Neutron Energy, E (MeV)
2-95
7884A6

Fig. 6

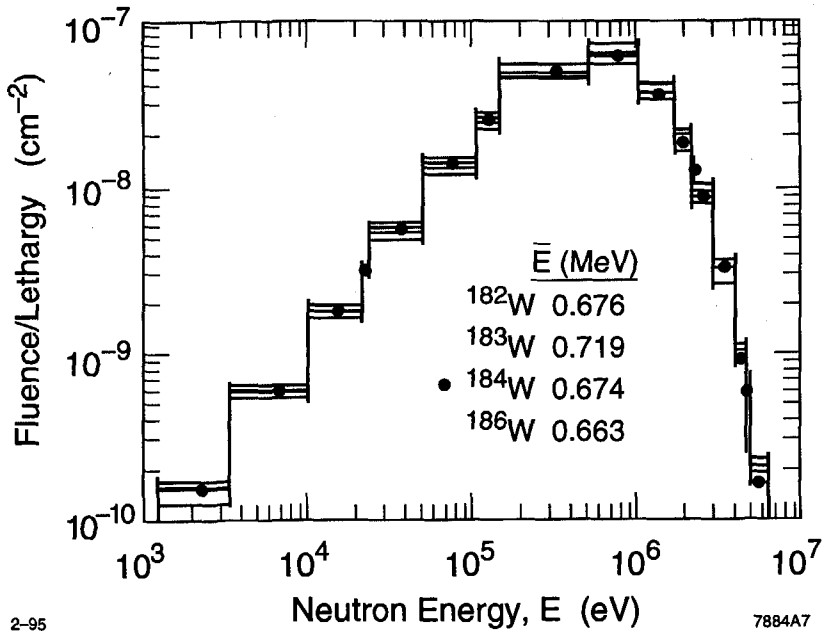
Fluence/Lethargy (cm^{-2})
10^{-7}
10^{-8}
10^{-9}
10^{-10}
10^3
10^4
10^5
10^6
10^7
Neutron Energy, E (eV)
$\bar{E}$ (MeV)
^{182}W 0.676
^{183}W 0.719
^{184}W 0.674
^{186}W 0.663
2-95
7884A7

Fig. 7

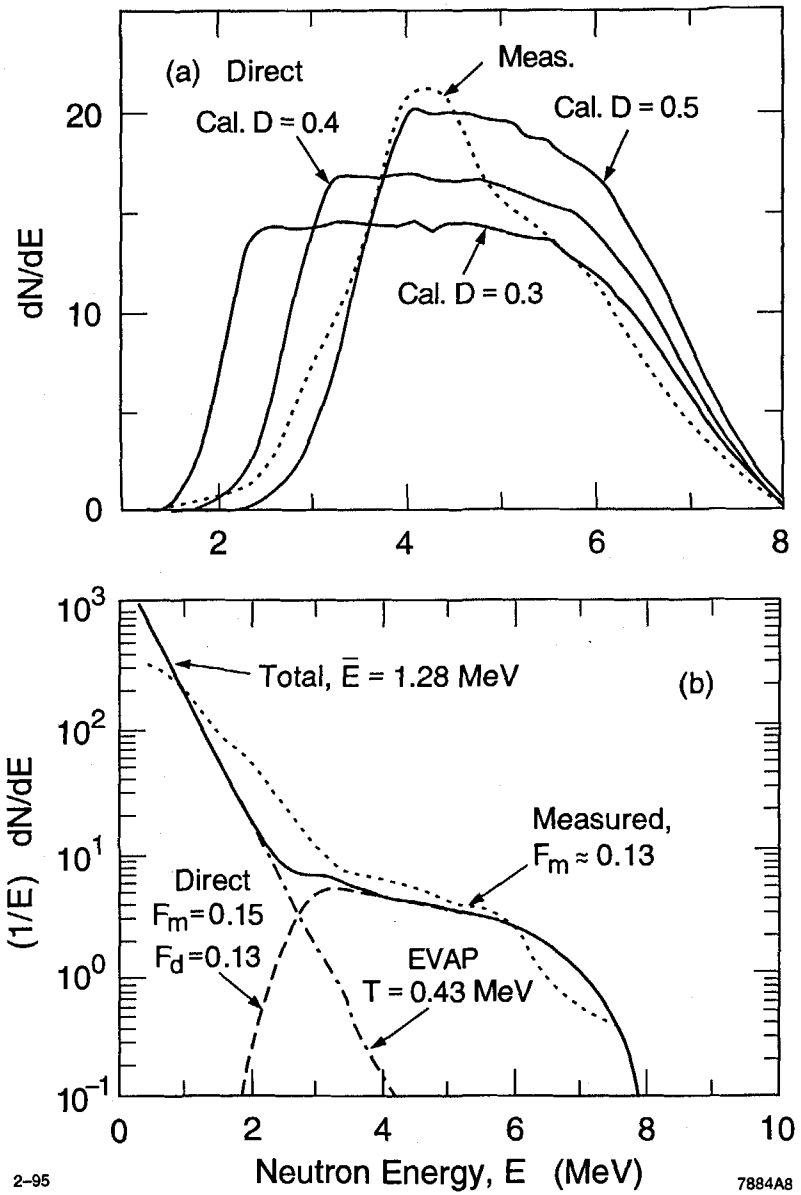
(a) Direct
Meas.
Cal. D = 0.4
Cal. D = 0.5
Cal. D = 0.3
dN/dE
20
10
0
2
4
6
8
Total, $\bar{E}$ = 1.28 MeV
(b)
Measured,
$F_m \approx 0.13$
Direct
F_m=0.15
F_d=0.13
EVAP
T = 0.43 MeV
(1/E) dN/dE
10^3
10^2
10^1
10^0
10^{-1}
0
2
4
6
8
10
Neutron Energy, E (MeV)
2-95
7884A8

Fig. 8

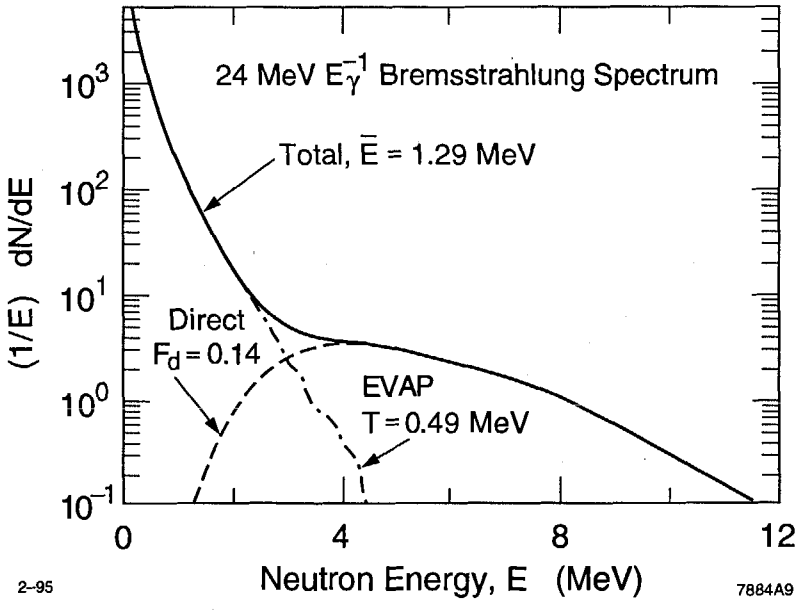
24 MeV E_γ^{-1} Bremsstrahlung Spectrum
Total, $\bar{E}$ = 1.29 MeV
Direct
F_d = 0.14
EVAP
T = 0.49 MeV
(1/E) dN/dE
Neutron Energy, E (MeV)
2-95
7884A9

Fig. 9

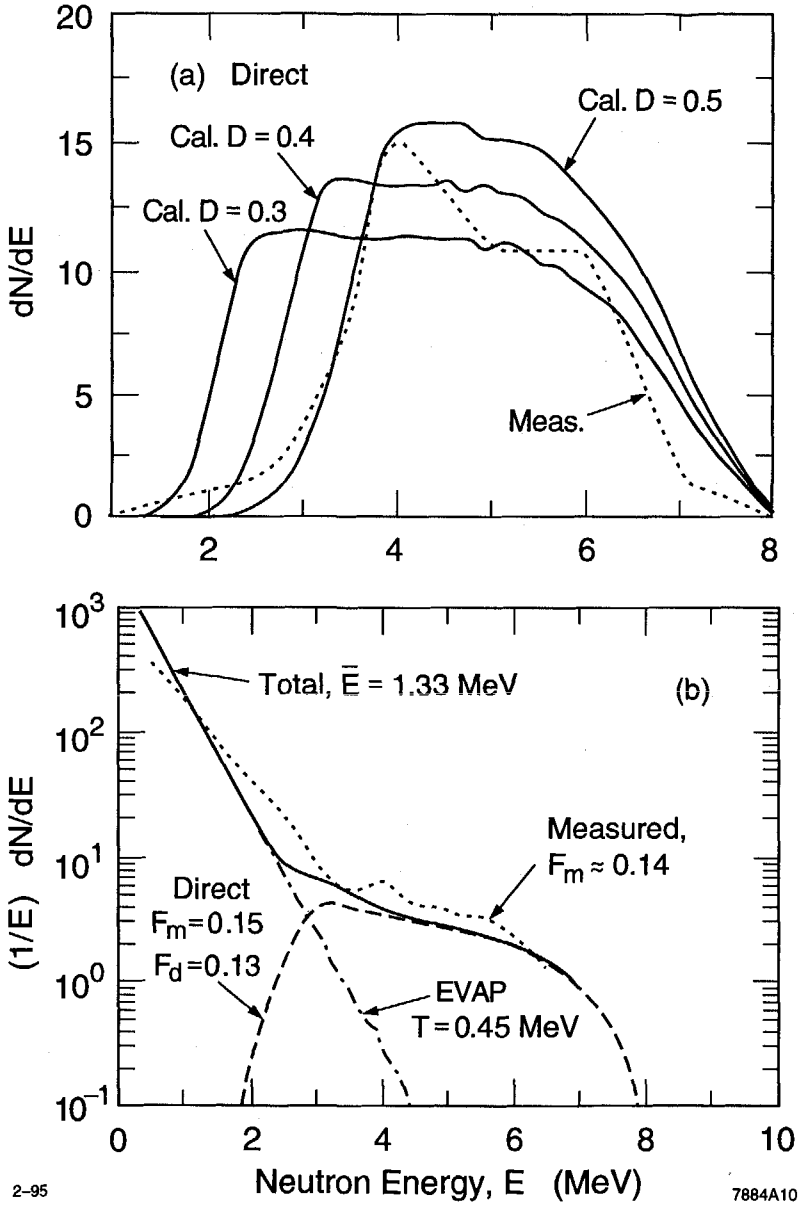
(a) Direct
Cal. D = 0.5
Cal. D = 0.4
Cal. D = 0.3
Meas.
dN/dE
Total, $\bar{E}$ = 1.33 MeV
(b)
Measured,
$F_m \approx 0.14$
Direct
F_m=0.15
F_d=0.13
EVAP
T = 0.45 MeV
(1/E) dN/dE
Neutron Energy, E (MeV)
2-95
7884A10

Fig. 10

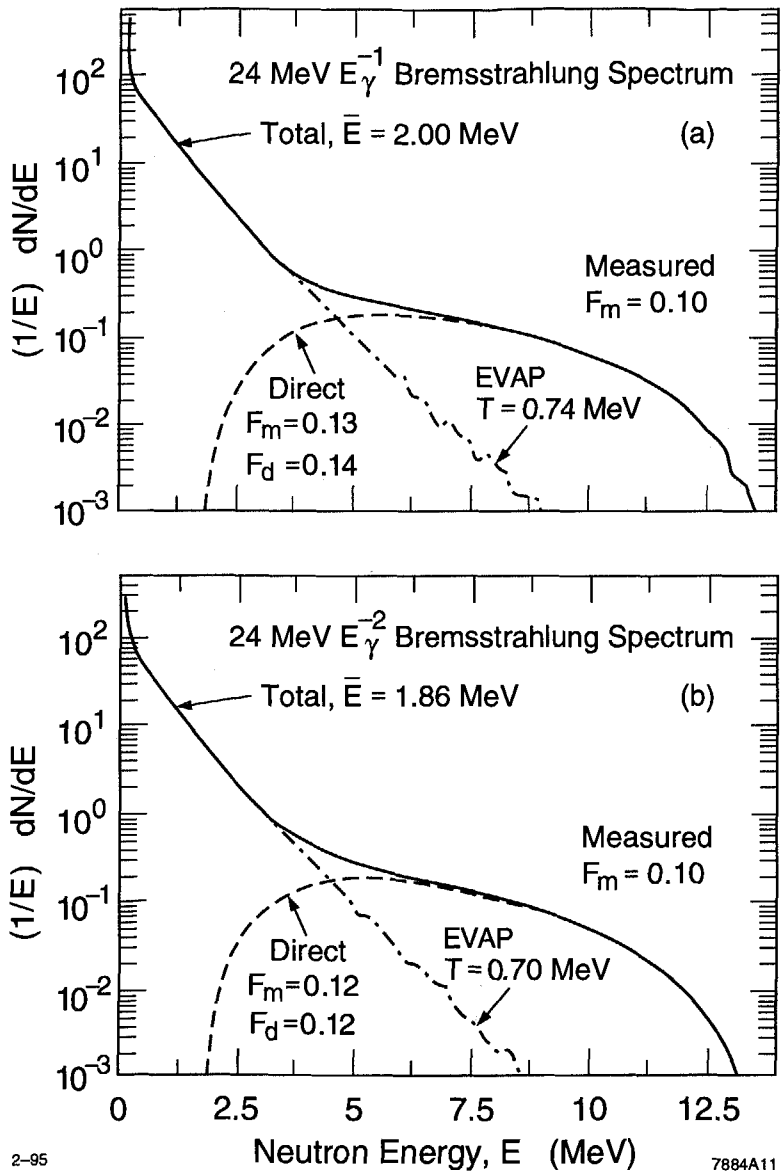
24 MeV E_γ^{-1} Bremsstrahlung Spectrum
Total, $\bar{E}$ = 2.00 MeV
(a)
Measured
F_m = 0.10
Direct
F_m=0.13
F_d =0.14
EVAP
T = 0.74 MeV
24 MeV E_γ^{-2} Bremsstrahlung Spectrum
Total, $\bar{E}$ = 1.86 MeV
(b)
Measured
F_m = 0.10
Direct
F_m=0.12
F_d=0.12
EVAP
T = 0.70 MeV
(1/E) dN/dE
10^2
10^1
10^0
10^{-1}
10^{-2}
10^{-3}
0
2.5
5
7.5
10
12.5
Neutron Energy, E (MeV)
2–95
7884A11

Fig. 11

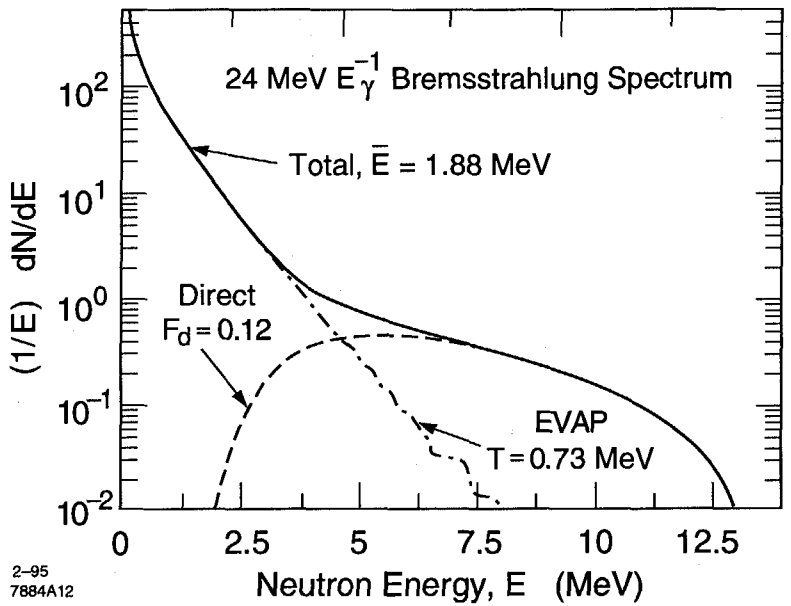
24 MeV E_γ^{-1} Bremsstrahlung Spectrum
Total, $\bar{E}$ = 1.88 MeV
Direct
F_d = 0.12
EVAP
T = 0.73 MeV
(1/E) dN/dE
10^2
10^1
10^0
10^{-1}
10^{-2}
0
2.5
5
7.5
10
12.5
Neutron Energy, E (MeV)
2–95
7884A12

Fig. 12